

# Basis Signal Optimization for $N$ -Continuous OFDM

Peng Wei, Yue Xiao, and Wei Xiang

**Abstract**—A novel basis signal optimization method is proposed for reducing the interference in the  $N$ -continuous orthogonal frequency division multiplexing (NC-OFDM) system. Compared to conventional NC-OFDM, the proposed scheme is capable of improving the transmission performance while maintaining an identical sidelobe suppression performance imposed by the linear combination of two groups of basis signals. Our performance results demonstrate that with a low complexity overhead, the proposed scheme is capable of striking a better trade-off among the bit error rate (BER), complexity, and the sidelobe suppression performance compared to its conventional counterpart.

**Index Terms**—Basis signal,  $N$ -continuous orthogonal frequency division multiplexing (NC-OFDM), sidelobe suppression.

## I. INTRODUCTION

Since the proposal of  $N$ -continuous orthogonal frequency division multiplexing (NC-OFDM) by Beek *et al.* [1], [2], sidelobe suppression based on the  $N$ -continuity criterion, where the signal is optimized to be continuous up to the  $N$ th-order derivative, has been developed as a class of frequency-domain precoders [1]–[7]. Although the  $N$ -continuity criterion has been widely employed for suppressing sidelobes, precoding in the frequency domain does not necessarily guarantee the direct elimination of self-interference in the multipath fading channel. For example, the self-interference caused by precoders in [1], [2] deteriorates the signal-to-noise ratio (SNR), so that selected mapping (SLM) [3] and cancellation tones [4] were proposed for mitigating the interference at the expense of complexity. By contrast, the family of self-interference reduction precoders [8], [9] were designed to directly reduce self-interference by adding precoder-induced interference in the guard interval, and hence, they are shown to outperform other counterparts in sidelobe suppression, complexity, and the bit error ratio (BER) performance. However, the interference added in the guard interval increases the sensitivity to channel-induced inter-symbol interference (ISI) and inter-carrier interference (ICI) [9]. Moreover, the precoder in [8] needs the information of the previous symbol which requires extra memory. In recent years, studies of time-domain precoding have found reduced-complexity applications in  $N$ -continuous OFDM [10], [11]. More specifically, in the aforementioned schemes, the linear combination-based  $N$ -continuous transmitter is designed with the aid of basis signals.

P. Wei is with the Department of Electronic Engineering, Beijing National Research Center for Information Science and Technology, Tsinghua University, Beijing 100084, China (e-mail: wppwwhttp@163.com).

P. Wei is also with the Tianjin Key Laboratory of Photoelectric Detection Technology and System and the School of Electronics and Information Engineering, Tiangong University, Tianjin 300387, China.

Y. Xiao is with the National Key Laboratory of Science and Technology on Communications, University of Electronic Science and Technology of China, Chengdu 611731, China (e-mail: xiaoyue@uestc.edu.cn).

W. Xiang is with the College of Science and Engineering, James Cook University, Cairns, Qld. 4878, Australia (e-mail: wei.xiang@jcu.edu.au).

Against the above background, the novel contribution of this paper is that a two linear-combination representations aided time-domain  $N$ -continuous OFDM scheme is proposed upon improving the continuities of the basis signals with the objective of adaptively controlling the self-interference without degrading its sidelobe suppression performance compared to conventional NC-OFDM.

## II. TIME-DOMAIN NC-OFDM

In this section, we give a brief introduction of time-domain NC-OFDM [10], [11], which with the given basis signals has an equivalent signal format as traditional NC-OFDM. In a baseband OFDM system, the input bit stream of the  $i$ th OFDM symbol is first modulated onto an uncorrelated complex-valued data vector  $\mathbf{d}_i = [d_{i,k_0}, d_{i,k_1}, \dots, d_{i,k_{K-1}}]^T$  drawn from a constellation such as phase-shift keying (PSK) or quadrature amplitude modulation (QAM). The complex-valued data vector is then mapped onto  $K$  subcarriers with the index set  $\mathcal{K} = \{k_0, k_1, \dots, k_{K-1}\}$ . Upon summing all the  $K$ -modulated orthogonal subcarriers with equal frequency spacing  $\Delta f = 1/T_s$ , the baseband OFDM signal is expressed as

$$x_i(t) = \sum_{r=0}^{K-1} d_{i,k_r} e^{j2\pi \frac{k_r}{T_s} t}, \quad (1)$$

where  $t \in \mathcal{T} \triangleq [-T_{cp}, T_s]$ ,  $T_s$  is the OFDM symbol duration, and  $T_{cp}$  denotes the length of the cyclic prefix (CP).

According to [10], [11] for time-domain  $N$ -continuous OFDM, a smooth signal  $\tilde{w}_i(t)$  is directly added to the CP-appended OFDM symbol  $x_i(t)$  for  $t \in \mathcal{T}$  to construct the  $N$ -continuous signal  $\bar{x}_i(t)$  given by

$$\bar{x}_i(t) = x_i(t) + \tilde{w}_i(t). \quad (2)$$

Aiming at eliminate discontinuities at the adjacent point indexed by  $-T_{cp}$  between two consecutive OFDM symbols as shown in Fig. 1,  $\tilde{w}_i(t)$  should follow

$$\tilde{w}_i^{(n)}(t) \Big|_{t=-T_{cp}} = \bar{x}_{i-1}^{(n)}(t) \Big|_{t=T_s} - x_i^{(n)}(t) \Big|_{t=-T_{cp}}, \quad (3)$$

where  $n \in \mathcal{U}_N \triangleq \{0, 1, \dots, N\}$  and  $x_i^{(n)}(t)$  represents the  $n$ th derivative of  $x_i(t)$ . Furthermore,  $\tilde{w}_i(t)$  is designed by linearly combining a group of basis signals  $f^{(n)}(t)$  as follows

$$\tilde{w}_i(t) = \sum_{n=0}^N b_{i,n} f^{(n)}(t), \quad (4)$$

where  $t \in \mathcal{T}$  and  $f^{(n)}(t)$  has the following design as

$$f^{(n)}(t) = \left( j \frac{2\pi}{T_s} \right)^n \sum_{k_r \in \mathcal{K}} k_r^n e^{j2\pi \frac{k_r}{T_s} (t+T_{cp})}. \quad (5)$$

Since the support length of  $f^{(n)}(t)$  is the same as that of  $x_i(t)$ , the interference caused by  $\tilde{w}_i(t)$ , existed in the whole OFDM symbol, results in severe performance degradation in BER. To solve this problem, an interference reduction design will be proposed via optimizing the basis signals.

### III. BASIS SIGNAL OPTIMIZED NC-OFDM

As illustrated in Fig. 1, by shortening the length of the smooth signal from  $T_s + T_{cp}$  to  $L$  ( $L < T_s + T_{cp}$ ), the optimized smooth signal  $w_i(t)$  is overlapped with  $x_i(t)$  according to (2) to construct the  $N$ -continuous signal  $\tilde{x}_i(t)$ .

Different from the traditional time-domain NC-OFDM system with discontinuities of  $x_i^{(n)}(t)$  for  $n \in \mathcal{U}_N$  at just one point, since the length of  $w_i(t)$  is smaller than that of  $x_i(t)$ , two disjoint points are required to be smoothed in the proposed scheme. As depicted in Fig. 1, the first one indexed by  $-T_{cp}$  and the second one indexed by  $T_L = -T_{cp} + L$  are introduced, which correspond to the beginning and end of  $w_i(t)$ , respectively. Thus, to meet the  $N$ -continuity criterion, the discontinuities at the two disjoint points are required to be smoothed at the same time.

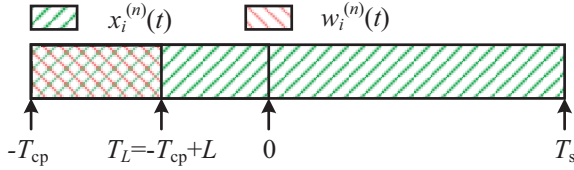


Fig. 1. Illustration of discontinuities of the derivatives of the low-interference  $N$ -continuous signal at two points in a baseband-equivalent OFDM symbol.

At time  $-T_{cp}$ , since the previous symbol  $x_{i-1}(t)$  is not affected by  $w_{i-1}(t)$ , for  $n \in \mathcal{U}_N$ ,  $w_i(t)$  should satisfy

$$w_i^{(n)}(t) \Big|_{t=-T_{cp}} = x_{i-1}^{(n)}(t) \Big|_{t=T_s} - x_i^{(n)}(t) \Big|_{t=-T_{cp}}. \quad (6)$$

Simultaneously, at time  $T_L$ , for the discontinuities caused by  $w_i^{(n)}(t)$  for  $n \in \mathcal{U}_N$ ,  $w_i(t)$  should satisfy

$$w_i^{(n)}(t) \Big|_{t=T_L} = 0. \quad (7)$$

Here we focus on designing  $w_i(t)$  satisfying (6) and (7). Inspired by (4), to eliminate the  $N + 1$  discontinuities at time  $-T_{cp}$  or  $T_L$ , each disjoint point requires at least  $N + 1$  basis signals. Thus, in our proposed scheme,  $w_i(t)$  including two linear combinations of two groups of basis signals is formulated as

$$w_i(t) = \begin{cases} \sum_{n=0}^N b_{i,n} f_n(t) + \sum_{\tilde{n}=0}^N \tilde{b}_{i,\tilde{n}} \tilde{f}_{\tilde{n}}(t), & t \in \mathcal{L}, \\ 0, & t \in \mathcal{T} - \mathcal{L}, \end{cases} \quad (8)$$

where the two linear combinations correspond to (6) and (7), respectively.  $\mathcal{L} \triangleq [-T_{cp}, T_L]$  indicates the range of  $w_i(t)$ , which implies that the self-interference caused by  $w_i(t)$  can be adaptively adjusted by  $L$ . Furthermore, the basis signals  $f_n(t)$  and  $\tilde{f}_{\tilde{n}}(t)$  are, respectively, designed as

$$f_n(t) = g_n(t) s_1(t), \quad (9)$$

$$\tilde{f}_{\tilde{n}}(t) = \tilde{g}_{\tilde{n}}(t) s_2(t), \quad (10)$$

which belong to basis sets  $\mathcal{Q}$  and  $\tilde{\mathcal{Q}}$ , respectively, as follows

$$\mathcal{Q} \triangleq \left\{ \mathbf{q}_n \mid \mathbf{q}_n = [f_n(-T_{cp}), \dots, f_n(T_L)]^T, n \in \mathcal{U}_N \right\}, \quad (11)$$

$$\tilde{\mathcal{Q}} \triangleq \left\{ \tilde{\mathbf{q}}_n \mid \tilde{\mathbf{q}}_n = [\tilde{f}_n(-T_{cp}), \dots, \tilde{f}_n(T_L)]^T, n \in \mathcal{U}_N \right\}, \quad (12)$$

where according to (5),  $g_n(t)$  and  $\tilde{g}_{\tilde{n}}(t)$  are given by

$$g_n(t) = f^{(n)}(t), \quad (13)$$

$$\tilde{g}_{\tilde{n}}(t) = f^{(n)}(t - L), \quad (14)$$

$s_1(t)$  and  $s_2(t)$  are the truncation windows.

It is noted that when a zero-edge window function  $s(t)$  whose first  $N_1$  derivatives are continuous is adopted as the truncation window, the continuities of  $f_n(t)$  and  $\tilde{f}_{\tilde{n}}(t)$  and their first  $N_1$  derivatives will be enhanced at the truncated points corresponding to the end and beginning of  $w_i(t)$ . This further smoothes the discontinuities of point  $w_i^{(n)}(T_L)$  for  $n = 0, 1, \dots, N_1$ . In this case, the number of discontinuities required to be removed at time  $T_L$  is reduced from  $N + 1$  to  $N - N_1$ . Thus, the condition (7) is changed to

$$w_i^{(n)}(t) \Big|_{t=T_L} = 0, n = N_1 + 1, \dots, N. \quad (15)$$

Subsequently, to remove the remaining  $N - N_1$  discontinuities, the design of  $w_i(t)$  in (8) is varied to

$$w_i(t) = \begin{cases} \sum_{n=0}^N b_{i,n} f_n(t) + \sum_{\tilde{n}=0}^{N-N_1-1} \tilde{b}_{i,\tilde{n}} \tilde{f}_{\tilde{n}}(t), & t \in \mathcal{L}, \\ 0, & t \in \mathcal{T} - \mathcal{L}. \end{cases} \quad (16)$$

Using the above  $s(t)$  for  $t \in [0, 2L]$  yields the truncation windows as

$$s_1(t) = s(t + T_{cp} + L) u(t + T_{cp}), t \in \mathcal{L}, \quad (17)$$

$$s_2(t) = s(t + T_{cp}) u(-t + |T_L|), t \in \mathcal{L}, \quad (18)$$

$s_1(t) = 0$  and  $s_2(t) = 0$  for  $t \notin \mathcal{L}$ , where  $u(t)$  is the unit step function. Actually,  $s_1(t)$  and  $s_2(t)$  correspond to the right and left halves of  $s(t)$ , respectively.

Then, based on the carefully designed  $f_n(t)$  and  $\tilde{f}_{\tilde{n}}(t)$ , coefficients  $b_{i,n}$  and  $\tilde{b}_{i,\tilde{n}}$  are calculated to generate  $w_i(t)$  as follows. Firstly, Eq. (16) is rewritten in matrix form as

$$\mathbf{w}_i = \mathbf{Q}_f \mathbf{b}_i + \mathbf{Q}_{\tilde{f}} \tilde{\mathbf{b}}_i, \quad (19)$$

where  $\mathbf{Q}_f = [\mathbf{q}_0 \ \mathbf{q}_1 \ \dots \ \mathbf{q}_N]$ ,  $\mathbf{Q}_{\tilde{f}} = [\tilde{\mathbf{q}}_0 \ \tilde{\mathbf{q}}_1 \ \dots \ \tilde{\mathbf{q}}_{N-N_1-1}]$ ,  $\mathbf{b}_i = [b_{i,0}, b_{i,1}, \dots, b_{i,N}]^T$ , and  $\tilde{\mathbf{b}}_i = [\tilde{b}_{i,0}, \tilde{b}_{i,1}, \dots, \tilde{b}_{i,N-N_1-1}]^T$ . Secondly, to satisfy both conditions (6) and (15), substituting (19) into (6) and (15) yields  $2N - N_1 + 1$  equations, expressed in the following matrix form

$$\begin{bmatrix} \mathbf{P}_f & \mathbf{P}_{\tilde{f}} \\ \mathbf{P}_{f_L} & \mathbf{P}_{\tilde{f}_L} \end{bmatrix} \begin{bmatrix} \mathbf{b}_i \\ \tilde{\mathbf{b}}_i \end{bmatrix} = \begin{bmatrix} \Delta \mathbf{x}_i \\ \mathbf{0}_{(N-N_1) \times 1} \end{bmatrix}, \quad (20)$$

where matrices  $\mathbf{P}_f$ ,  $\mathbf{P}_{\tilde{f}}$ ,  $\mathbf{P}_{f_L}$ , and  $\mathbf{P}_{\tilde{f}_L}$  are, respectively, defined as  $[\mathbf{P}_{f_L}]_{\tilde{n}+1, \tilde{n}+1} = f_{\tilde{n}}^{(\tilde{n}+N_1+1)}(T_L)$ ,  $[\mathbf{P}_f]_{n+1, \tilde{n}+1} = f_n^{(n)}(-T_{cp})$ ,  $[\mathbf{P}_{\tilde{f}}]_{n+1, \tilde{n}+1} = \tilde{f}_{\tilde{n}}^{(n)}(-T_{cp})$ ,  $[\mathbf{P}_{\tilde{f}_L}]_{\tilde{n}+1, \tilde{n}+1} = \tilde{f}_{\tilde{n}}^{(\tilde{n})}(T_L)$  for  $n, \tilde{n} \in \mathcal{U}_N$  and  $\tilde{n}, \hat{n} \in \mathcal{U}_{N-N_1-1}$ , and  $\Delta \mathbf{x}_i$  is an  $(N+1) \times 1$  vector of the differences between  $\mathbf{x}_i$  and  $\mathbf{x}_{i-1}$ ,

as well as their first  $N$  derivatives at time  $-T_{cp}$ , which can be calculated by

$$\Delta \mathbf{x}_i = \mathbf{P}_1 \mathbf{d}_{i-1} - \mathbf{P}_2 \mathbf{d}_i, \quad (21)$$

where  $[\mathbf{P}_1]_{n+1,r+1} = \frac{(j2\pi k_r)^n}{T_s^n}$ ,  $\mathbf{P}_2 = \mathbf{P}_1 \Phi$ ,  $\Phi \triangleq \text{diag}(e^{j\varphi k_0}, e^{j\varphi k_1}, \dots, e^{j\varphi k_{K-1}})$ , and  $\varphi = -2\pi T_{cp}/T_s$ . Lastly,

when the rank of the coefficient matrix  $\begin{bmatrix} \mathbf{P}_f & \mathbf{P}_{\tilde{f}} \\ \mathbf{P}_{f_L} & \mathbf{P}_{\tilde{f}_L} \end{bmatrix}$  is equal to that of the augmented matrix  $\begin{bmatrix} \mathbf{P}_f & \mathbf{P}_{\tilde{f}} & \Delta \mathbf{x}_i \\ \mathbf{P}_{f_L} & \mathbf{P}_{\tilde{f}_L} & \mathbf{0}_{(N-N_1) \times 1} \end{bmatrix}$  in (20), if the coefficient matrix is of full rank, the coefficient vectors can be derived as

$$\begin{bmatrix} \mathbf{b}_i \\ \tilde{\mathbf{b}}_i \end{bmatrix} = \begin{bmatrix} \mathbf{P}_f & \mathbf{P}_{\tilde{f}} \\ \mathbf{P}_{f_L} & \mathbf{P}_{\tilde{f}_L} \end{bmatrix}^{-1} \begin{bmatrix} \mathbf{P}_1 \mathbf{d}_{i-1} - \mathbf{P}_2 \mathbf{d}_i \\ \mathbf{0}_{(N-N_1) \times 1} \end{bmatrix} \quad (22)$$

$$= \mathbf{P} (\mathbf{P}_1 \mathbf{d}_{i-1} - \mathbf{P}_2 \mathbf{d}_i), \quad (23)$$

where  $\mathbf{P}$  is composed of the first  $N+1$  columns of  $\begin{bmatrix} \mathbf{P}_f & \mathbf{P}_{\tilde{f}} \\ \mathbf{P}_{f_L} & \mathbf{P}_{\tilde{f}_L} \end{bmatrix}^{-1}$ . It is noted that when the rank of the coefficient matrix is smaller than  $2N - N_1 + 1$  and equal to that of the augmented matrix, there will be infinite solutions in (20). In this case, the inverse of the coefficient matrix in (22) is changed to the Moore-Penrose pseudo-inverse for a minimum Euclidean-norm solution.

Finally, it follows from (2), (19), and (23) that the  $N$ -continuous symbol  $\tilde{\mathbf{x}}_i$  is expressed as

$$\tilde{\mathbf{x}}_i = \begin{cases} \mathbf{x}_i + \begin{bmatrix} [\mathbf{Q}_f & \mathbf{Q}_{\tilde{f}}] \mathbf{P} (\mathbf{P}_1 \mathbf{d}_{i-1} - \mathbf{P}_2 \mathbf{d}_i) \\ \mathbf{0}_{(T_s + T_{cp} - L) \times 1} \end{bmatrix}, & 0 \leq i \leq M_s - 1, \\ [\mathbf{Q}_f & \mathbf{Q}_{\tilde{f}}] \mathbf{P} (\mathbf{P}_1 \mathbf{d}_{i-1} - \mathbf{P}_2 \mathbf{d}_i), & i = M_s, \end{cases} \quad (24)$$

where  $M_s$  is the number of consecutive OFDM symbols, and  $\mathbf{d}_{-1}$  is initialized as a zero vector  $\mathbf{d}_{-1} = \mathbf{0}_{K \times 1}$ .

#### IV. SIMULATION RESULTS

TABLE I  
SIMULATION PARAMETERS

Parameters	Values
Constellation modulation	16QAM
Number of subcarriers ( $K$ )	256
Subcarrier index set ( $\mathcal{K}$ )	$\{-128, -127, \dots, 127\}$
OFDM symbol duration ( $T_s$ )	1/15 ms
Sampling interval ( $T_{\text{samp}}$ )	$T_s/2048$
Frequency interval ( $\Delta f$ )	15 KHz
Carrier frequency	2 GHz
Maximum Doppler shift ( $f_D$ )	111.11 Hz
CP length in OFDM ( $T_{cp}$ )	$144 T_{\text{samp}}$
Window function ( $s(t)$ )	Blackman window

We show our performance results employing the simulation parameters listed in Table I, where since the Blackman window and its first derivative are continuous, we have  $N_1 = 1$ . For comparison, the performance of original OFDM, conventional NC-OFDM [1], prefix precoding [8], and prefix/suffix precoding [9] is also considered, where the lengths of the prefix and suffix are set to 72 in the prefix/suffix precoding [9]. To demonstrate the performance of sidelobe suppression, the power spectrum density (PSD) is evaluated by Welch's

averaged periodogram method with a 2048-sample Hanning window and 512-sample overlap after observing  $10^5$  symbols.

Fig. 2 depicts the sidelobe suppression performances of original OFDM, conventional NC-OFDM, the prefix precoding, the prefix/suffix precoding, and the proposed scheme, where we set  $N=0,2,4,6$  and  $L=72,144,1024$ . As can be observed, when  $N$  is big, all the  $N$ -continuous schemes have a significant reduction in out-of-band emission as opposed to OFDM, where NC-OFDM has the best performance gain. More importantly, by increasing  $L$ , the performance of our proposed scheme becomes approaching that of NC-OFDM. To specify this case, in Table II, we further calculate all the curves in Fig. 2 in terms of the adjacent channel leakage power ratio (ACLR), which is defined as the ratio of the average power in band B0 to the average power outside of band B0 [12], where ACLR1 and ACLR2 are associated with band B1 close to B0 and band B2 far from B0, respectively. The results are calculated upon the bandwidth of B0 equal to that of B1 and equal to that of B2. It can be observed that the ACLR of the proposed scheme is close to that of NC-OFDM for small  $L$ , such as  $L=72$ , namely the  $N$ -continuity is well ensured by the proposed scheme with a short-length smooth signal.

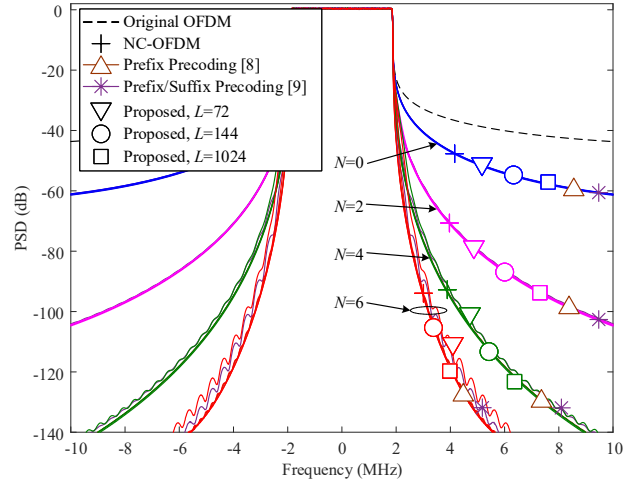


Fig. 2. PSD comparison of OFDM, NC-OFDM, prefix precoding, prefix/suffix precoding, and the proposed scheme with different  $N$  and  $L$ .

TABLE II  
NUMERICAL RESULTS OF ACLR CORRESPONDING TO FIG. 2

Scheme	ACLR1 (dB)	ACLR2 (dB)
<b>OFDM</b>	34	42
<b>NC-OFDM, Precoding [8], Precoding [9]</b>	$N=0$	40, 40, 40
	$N=2$	51, 50, 50
	$N=4$	61, 60, 58
	$N=6$	70, 68, 65
<b>Proposed</b>	$L=72$	40, 40, 40
	$L=144$	48, 51, 51
	$L=1024$	50, 58, 60
	$L=1024$	52, 62, 70

Fig. 3 plots the BERs of the proposed scheme and its counterparts in the multipath fading channel with the channel tap delay [0, 30, 150, 310, 370, 710, 1090, 1730, 2510] ns and the channel relative power [0, -1.5, -1.4, -3.6, -0.6, -9.1, -7, -12, -16.9] dB [13]. Furthermore, perfect channel information is

assumed at the receiver and zero-forcing channel equalization is adopted. The proposed scheme exhibits promising BER results, which are close to those of conventional OFDM, while the NC-OFDM receiver exhibits a worse performance for big  $N$ , such as  $N=6$ . Even if a recovery processing [1] with 8 iterations is considered, the floor emerges at  $E_b/N_0=35$  dB. In the low  $E_b/N_0$  region, the precoding schemes in [8], [9] exhibit the identical error performance to OFDM. On the contrary, when  $E_b/N_0$  is higher, since the introduced interference in [8], [9] has the same duration as the guard interval, the BER performance of the precoding schemes in [8], [9] is negatively influenced by the channel-delayed self-interference for big  $N$ , such as  $N=6$  at  $E_b/N_0=35$  dB. It can be also inferred that the proposed scheme's performance is not affected by the smooth signal, owing to the fact that the proposed scheme is capable of adaptively reducing the length of the smooth signal so that the channel-delayed smooth signal cannot interfere with the useful signal.

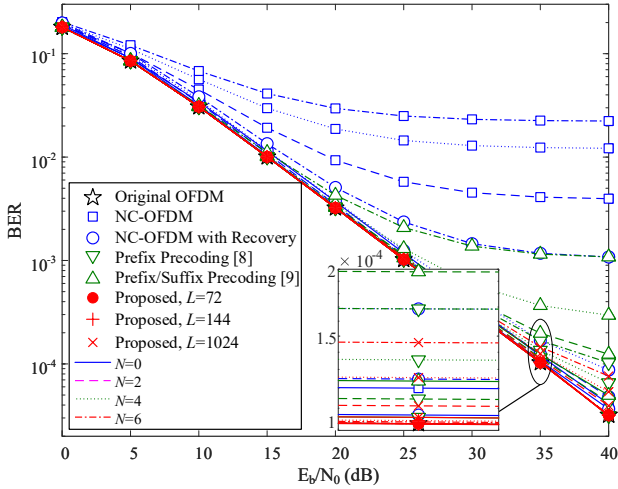


Fig. 3. BERs of OFDM, NC-OFDM, prefix precoding, prefix/suffix precoding, and the proposed scheme with different  $N$  and  $L$ .

In Table III, compared to original OFDM, we further compute the additional complexity and the required memory of the proposed scheme and its counterparts, which are, respectively, measured by the number of complex multiplications and the number of memory units for complex data. As shown in Figs. 2 and 3 and Table II, the proposed scheme is capable of achieving promising sidelobe suppression and BER performance for the  $L$  much smaller than  $K=256$  (e.g.,  $L=144$ ). In this case, it can be calculated from Table III that when  $N = 4$  and  $N_1 = 1$ , the complexity ratios of the proposed scheme to NC-OFDM, prefix precoding [8], and prefix/suffix precoding [9] are 96.56%, 60.49%, and 45.37%, respectively. Furthermore, the proposed scheme just requires  $N+1$  units of memories for storing  $\mathbf{P}_1 \mathbf{d}_{i-1}$  to calculate  $\Delta \mathbf{x}_i$ , which are much smaller than that in [1], [8] and slightly higher than that in [9].

Furthermore, Fig. 4 plots the power ratio of the smooth signal over the OFDM signal in the proposed scheme as opposed to its counterparts. It can be seen that for a small  $L$ , the proposed scheme consumes much lower power than the precoders in [8], [9]. As  $L$  increases to a value bigger than  $T_{cp}$ ,

the power consumed by the proposed scheme also increases but is still less than those of the precoders in [8], [9], especially for a large  $N$ . Fig. 5 further confirms the conclusion taken by Fig. 4, where the power ratio of the smooth signal over the initial  $L$  useful OFDM samples in the proposed scheme is investigated and compared.

TABLE III  
ADDITIONAL COMPLEXITY AND MEMORY OF VARIOUS  $N$ -CONTINUOUS SCHEMES COMPARED TO ORIGINAL OFDM

Scheme	Additional number of complex multiplications	Additional number of memory
NC-OFDM	$4(N+1)K$	$K$
Precoding [8]	$8(N+1)K$	$K$
Precoding [9]	$6(N+1)K$	0
Proposed	$2(N+1)K + 2(2N+1-N_1)(L+N+1)$	$N+1$

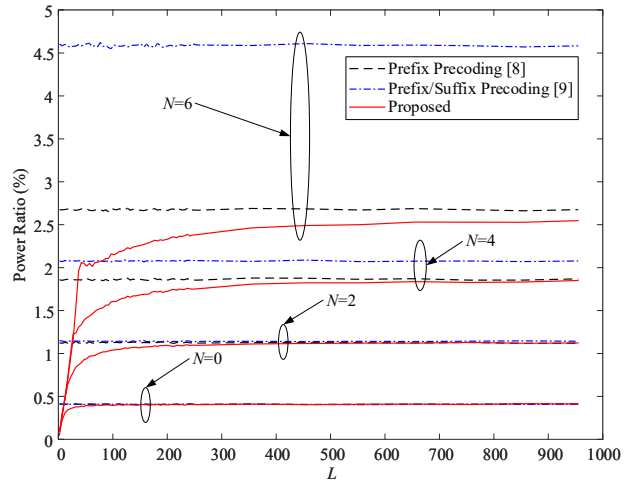


Fig. 4. Power ratio of the interference at the transmitter in prefix precoding, prefix/suffix precoding, and the proposed scheme with different  $N$  and  $L$ .

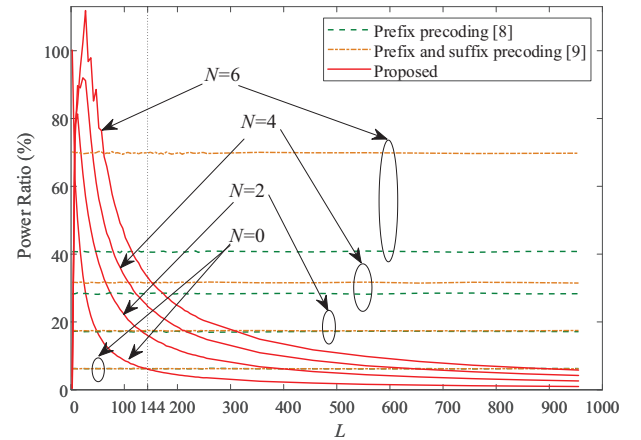


Fig. 5. Power ratio of the interference over the OFDM signal in the initial  $L$  samples in the proposed scheme.

## V. CONCLUSION

In this paper, we proposed a class of novel  $N$ -continuous OFDM schemes designed for interference cancellation,

through enhancing the continuities of the basis signals and their higher-order derivatives. Our simulation results revealed that the proposed scheme outperforms its counterparts in the trade-off among sidelobe suppression, computational complexity and BER performance.

#### REFERENCES

- [1] J. van de Beek and F. Berggren, “ $N$ -continuous OFDM,” *IEEE Commun. Lett.*, vol. 13, no. 1, pp. 1-3, Jan. 2009.
- [2] J. van de Beek and F. Berggren, “Out-of-band power suppression in OFDM,” *IEEE Commun. Lett.*, vol. 12, no. 9, pp. 609-611, Sep. 2008.
- [3] M. Ohta, A. Iwase, and K. Yamashita, “Improvement of the error characteristics of an  $N$ -continuous OFDM system with low data channels by SLM,” in *Proc. IEEE Int. Conf. Commun. (ICC)*, Kyoto, Japan, Jun. 2011, pp. 1-5.
- [4] M. Ohta, M. Okuno, and K. Yamashita, “Receiver iteration reduction of an  $N$ -continuous OFDM system with cancellation tones,” in *Proc. IEEE Glob. Telecommun. Conf. (GLOBECOM)*, Kathmandu, Nepal, Dec. 2011, pp. 1-5.
- [5] H. Kawasaki, M. Ohta, and K. Yamashita, “Extension of  $N$ -continuous OFDM precoder matrix for improving error rate,” *IEEE Commun. Lett.*, vol. 19, no. 2, pp. 283-286, Feb. 2015.
- [6] M. Mohamad, R. Nilsson, and J. van de Beek, “Minimum-EVM  $N$ -continuous OFDM,” in *Proc. IEEE Int. Conf. Commun. (ICC)*, Kuala Lumpur, Malaysia, May 2016, pp. 1-5.
- [7] R.-A. Pitaval, B. M. Popović, and J. van de Beek, “ $N$ -continuous SC-FDMA and its polarized transmission and reception,” *IEEE Trans. Commun.*, vol. 65, no. 11, pp. 4911-4925, Nov. 2017.
- [8] H. Kawasaki, M. Ohta, and K. Yamashita, “ $N$ -continuous symbol padding OFDM for sidelobe suppression,” in *Proc. IEEE Int. Conf. Commun. (ICC)*, Sydney, Australia, Jun. 2014, pp. 5890-5895.
- [9] T. Taheri, R. Nilsson, and J. van de Beek, “Quasi-cyclic symbol extensions for shaping the OFDM spectrum,” *IEEE Trans. Wireless Commun.*, vol. 17, no. 10, pp. 7054-7066, Oct. 2018.
- [10] P. Wei, L. Dan, Y. Xiao, and S. Li, “A low-complexity time-domain signal processing algorithm for  $N$ -continuous OFDM,” in *Proc. IEEE Int. Conf. Commun. (ICC)*, Budapest, Hungary, Jun. 2013, pp. 5754-5758.
- [11] P. Wei, L. Dan, Y. Xiao, W. Xiang, and S. Li, “Time-domain  $N$ -continuous OFDM: System architecture and performance analysis,” *IEEE Trans. Veh. Technol.*, vol. 66, no. 3, pp. 2394-2407, Mar. 2017.
- [12] *E-UTRA RF system scenarios Radio Frequency (RF) system scenarios (Release 15)*, 3GPP TR 36.942, v15.0.0, Jun. 2018. [Online]. Available: <http://www.3gpp.org/>.
- [13] *E-UTRA Base Station (BS) radio transmission and reception (Release 15)*, 3GPP TS 36.104, v15.4.0, Sep. 2018. [Online]. Available: <http://www.3gpp.org/>.